Rule-based Control and Equivalent Consumption Minimization Strategies for Hybrid Electric Vehicle Powertrains: a Hardware-in-the-loop Assessment

Rule-based Control and Equivalent Consumption Minimization Strategies for Hybrid Electric Vehicle Powertrains: a Hardware-in-the-loop Assessment

Pier Giuseppe Anselma
[1]*Department of Mechanical and Aerospace Engineering (DIMEAS), Politecnico di Torino*
Torino, Italy
[2]*Center for Automotive Research and Sustainable Mobility (CARS), Politecnico di Torino*
Torino, Italy
pier.anselma@polito.it

***Abstract*—Energy management systems are crucial in hybrid electric vehicles (HEVs). Other than enhanced energy economy, a proper energy management system must guarantee acceptable driving comfort, compliance with the allowed battery state-of-charge window, and on-board computational efficiency. While several studies from the literature have compared different state-of-the-art real-time HEV powertrain energy management strategies, not much work has been performed on the hardware-in-the-loop (HIL) assessment of these control approaches. This paper aims at answering the identified research need by performing an experimental HIL assessment of different state-of-the-art HEV control strategies including a rule-based control (RBC) approach and three different formulations of equivalent consumption minimization strategy (ECMS), both of traditional and adaptive type. A parallel-through-the-road HEV is considered for this case study. Various assessment criteria are retained including HEV fuel economy, measured computational time, and comfort of the ride in terms of frequency of de/activation events and smoothness of the controlled value of torque over time for the internal combustion engine. Obtained results suggest that the RBC approach can achieve improved performance in almost all the retained evaluation criteria. The traditional ECMS can outperform RBC in terms of fuel economy, yet by undermining both ride comfort and compliance with the battery SOC window. Finally, an adaptive ECMS can outperform the RBC in terms of fuel economy while ensuring acceptable comfort and compliance with the battery SOC window, yet at a significant computational cost increase.**

Keywords—energy management, fuel economy, hardware-in-the-loop (HIL), hybrid electric vehicle (HEV), real-time control

I. Introduction

Hybrid electric vehicles (HEVs) can achieve significantly less tailpipe emissions than conventional internal combustion engine (ICE) vehicles, and HEVs are conveniently not dependent on charging infrastructure like pure electric vehicles. However, HEVs pose new challenges in appropriately coordinating the ICE and the electric motor/generators (EMs). Energy management systems are thus developed to maximize HEV energy economy while guaranteeing enhanced comfort of the ride and ease of on-board implementation [1]. Real-time implementable control approaches for HEV powertrains are notably divided into three main categories: 1) heuristic, 2) instantaneous optimization based, and 3) artificial intelligence based [2]. Typical examples of heuristic HEV energy management approaches include rule-based methods and fuzzy logics. On the other hand, equivalent consumption minimization strategy (ECMS) is the most popular instantaneous optimization HEV powertrain control approach. Finally, artificial intelligence HEV control strategies include a variety of approaches from supervised learning to deep reinforcement learning [3].

The above-mentioned real-time control approaches yield different HEV powertrain operation over time which can be evaluated according to various metrics such as HEV energy economy and comfort of the ride for example. Few research works in the literature have compared different HEV control approaches based on numerical simulations. In general, ECMS was found achieving higher HEV fuel economy potential compared with a rule-based approach [4]. Nevertheless, ECMS typically entails more frequent ICE de/activations over time, which can undermine passenger comfort [5]. As the research regarding effective HEV real-time control advances, comparative studies should focus also on practical implementation aspects such as the required on-board computational power and the control algorithm execution time for example. Hardware-in-the-loop (HIL) simulations are required to this end. In 2015, Mura et al. compared an adaptive ECMS (A-ECMS) with a nonlinear optimization control strategy and implemented the HEV control algorithms on an HIL simulation platform [6]. In 2016, Hartavi et al. validated a rule based HEV control approach on a HIL simulator [7]. In 2019, Herrera et al. benchmarked a predictive fuzzy logic with a heuristic control strategy for a hybrid electric bus using a HIL test-bench [8]. Nevertheless, none of the reviewed studies benchmarked HEV control strategies in terms of on-board practical aspects such as computational power and execution time for example. As consequence, more research is required to thoroughly assess different HEV control approaches from the literature. This paper aims at partially filling the identified research gap by performing a HIL assessment of a rule-based control (RBC) approach and three formulations of ECMS for a HEV powertrain. Several evaluation metrics are considered including HEV fuel economy, comfort of the ride in terms of frequency of ICE de/activations and ICE torque smoothness over time, and computational power demand. The rest of this paper is organized as follows: the retained HEV plant model and control strategies are described first. Then, the considered

HIL platform is illustrated and obtained results are discussed. Conclusions are finally given.

II. HEV Simulation Platform and Plant Model

This section illustrates the HEV powertrain architecture under study first, and subsequently describes the simulation platform implemented.

A. HEV Powertrain Architecture

Fig. 1 shows the considered HEV powertrain layout, namely a parallel P4 or parallel-through-the-road architecture. In this HEV, the ICE propels the front axle through a six-speed automated manual transmission (AMT). On the other hand, the EM powers the rear axle by means of a direct drive transmission and it is linked to the high-voltage battery pack. The torques of the ICE and the EM are added at the road level.

TABLE I reports HEV data considered in this paper, which have been inspired by the commercially available Jeep Renegade 4xe [9]. In particular, road load (RL) coefficients have been retained from the US Environmental Protection Agency (EPA) database [10]. On the other hand, operating maps for ICE, EM and battery have been numerically generated by means of the methodology implemented in Simcenter Amesim® software [11].

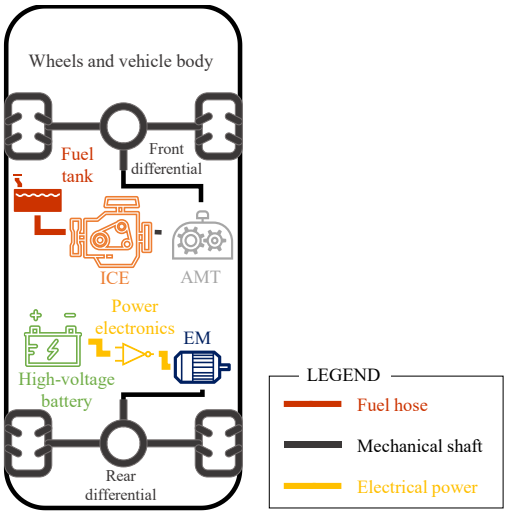

Fig. 1. Schematic diagram of the retained parallel-through-the-road HEV powertrain architecture.

TABLE I. Retained HEV Data

Component	Parameter	Value
Vehicle body	Equivalent mass [kg]	2120
	RL_A [N]	125.22
	RL_B [N/(m/s)]	1.95
	RL_C [N/(m/s)^2]	0.59
	Wheel radius [m]	0.29
AMT	Gear ratios	[4.46 2.51 1.56 1.14 0.85 0.67]
	Front differential ratio	3.68
	Rear differential ratio	5.60
ICE	Type	Spark-ignition, Turbocharged
	Capacity [L]	1.4
	Max power [kW @ rpm]	133 @ 5750
	Max torque [Nm @ rpm]	270 @ 1850
EM	Max power [kW]	44
	Max torque [Nm]	250
Battery pack	Celll type and configuration	Nickel Manganese Cobalt (NMC), 109S 1P
	Nominal voltage [V]	400
	Cell capacity [Ah]	28.4

B. HEV Simulation Platform

The HEV simulation platform considered in this work is illustrated in Fig. 2 and implemented in Matlab/Simulink® software. In particular, the vehicle speed profile for the target drive cycle is fed to a proportional–integral–derivative (PID) controller which emulates the driver. The driver compares the target vehicle speed value with the actual vehicle speed value as provided by the HEV plant model, and it consequently evaluates a value of demanded torque. The computed overall torque demand is then fed to the HEV controller, which is responsible for operating two HEV powertrain control decisions: 1) the gear number to be engaged, and 2) the torque split between ICE and EM. The gear number to be engaged by the AMT is selected using a lookup table based on the instantaneous value of vehicle speed as provided by the HEV plant model. On the other hand, commanded values of torque for both ICE and EM are decided by the HEV energy management system using one of the control logics which will be detailed in the next section based on various vehicle states including speed of power components and battery state-of-charge (SOC) for example. The generated powertrain control signals are then sent to the HEV plant model, which updates the instantaneous vehicle states and closes the control loop by providing feedback information to the driver and to the HEV controller. The next section will provide further details regarding the considered HEV plant model.

C. HEV Plant model

In general, only longitudinal vehicle dynamics are considered here, and the vehicle chassis is modelled as a single equivalent mass using (1):

$$\frac{T_{wheels}}{r_{wheel}} = \left[RL_A \cdot sign(v_x) + RL_B \cdot v_x + RL_C \cdot v_x^2 + m_{eq} \cdot a_x\right] \quad (1)$$

where T_{wheels} and r_{wheel} are the total torque of the power components at the wheel level and the wheel dynamic radius, respectively. v_x and a_x stand for longitudinal speed and acceleration of the vehicle, respectively. m_{eq} is the HEV equivalent mass which considers the equivalent mass of rotating components of the powertrain as well. Finally, RL_A, RL_B and RL_C are empirical coefficients which model the vehicle road load as a function of the longitudinal vehicle

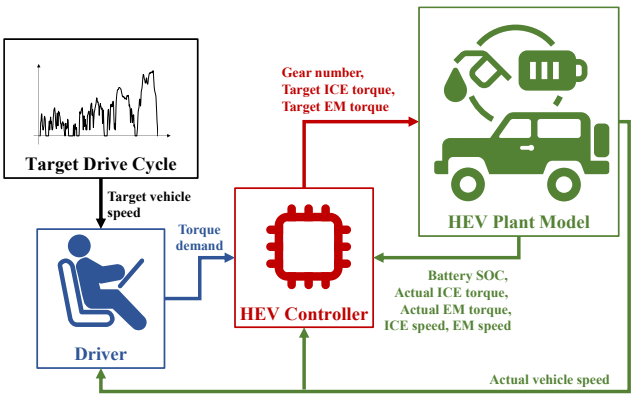

Fig. 2. HEV simualtion platform implemented in this work.

speed and that consider different contributions such as aerodynamic drag and rolling resistance for example.

Speeds of power components can be directly evaluated from the vehicle speed. Moreover, the torque balance at the wheels at each time instant can be expressed as follows:

$$T_{wheels} = T_{ICE} \cdot \tau_{AMT}(gear) \cdot \tau_{diff-front} \cdot \eta_{AMT} \cdot \eta_{diff-front} + T_{EM} \cdot \tau_{diff-rear} \cdot \eta_{diff-rear}^{sign(T_{EM})} \quad (2)$$

where T_{ICE} and T_{EM} are the ICE torque and the EM torque, respectively. Ratios of the engaged gear number in the AMT ($gear$), of the front axle differential and of the rear axle differential are respectively denoted by $\tau_{AMT}(gear)$, $\tau_{diff-front}$ and $\tau_{diff-rear}$. Finally, η_{AMT}, $\eta_{diff-front}$, and $\eta_{diff-rear}$ stand for mechanical efficiencies of the AMT, the front axle differential and the rear axle differential, respectively. Considering the sign of the EM torque as power factor of the rear differential efficiency allows retaining both propelling and generating cases.

As concerns the electrical energy path, the amount of power that the battery is requested to either deliver or absorb (P_{batt}) can be determined as:

$$P_{batt} = \frac{P_{EM}}{[\eta_{EM}(\omega_{EM}, T_{EM})]^{sign(P_{EM})}} \quad (3)$$

where P_{EM} and η_{EM} respectively denote the mechanical power and the overall efficiency of the EM. The latter is evaluated by means of an empirical lookup table with speed (ω_{EM}) and torque (T_{EM}) as independent variables. Retaining the sign of P_{EM} as exponent in the denominator allows capturing both depleting and charging battery conditions within this formula. The rate of battery SOC ($\dot{SOC}$) can then be evaluated by considering an equivalent open circuit model as in equation (4):

$$\dot{SOC} = \frac{I_{batt}}{As_{batt}} = \frac{V_{OC}(SOC) - \sqrt{[V_{OC}(SOC)]^2 - 4 \cdot R_{IN}(SOC) \cdot P_{batt}}}{2 \cdot R_{IN}(SOC) \cdot As_{batt}} \quad (4)$$

where V_{OC} and R_{IN} are the open-circuit voltage and the internal resistance of the battery pack, as obtained by interpolating in one dimensional lookup tables with SOC ad independent variable. I_{batt} is the battery pack current, while As_{batt} is the battery pack capacity in ampere-seconds.

Concerning the ICE, the instantaneous mass flow rate of fuel in grams per second $\dot{m}_{fuel}$ can be evaluated using an empirical steady-state lookup table with torque and speed as independent input variables. Furthermore, instantaneous variations in the value of ICE torque are saturated in the HEV plant model within 50 Nm/s and -100 Nm/s. Such values have been selected based on engineering thought, and they aim to reproduce the physical limitations of a real ICE.

III. HEV Control Strategies

This section illustrates the operating principle of the implemented real-time HEV control strategies including RBC, ECMS, and two versions of A-ECMS.

A. RBC

The RBC strategy implemented in this work is based off the charge-sustaining energy management strategy for several commercially available HEV powertrains and includes control of the ICE state and of the ICE torque [12]. The ICE state is set to on if either the battery SOC is below a given lower threshold SOC_{low} or the requested wheel power is above an upper threshold P_{up} which cannot be supplied by the battery pack alone. The ICE is kept on until either the battery SOC exceeds a given upper threshold SOC_{up} or the requested wheel power is lower than a certain threshold P_{low}. Different upper and lower threshold values are used to reduce the frequency of ICE activations. After the first cranking event in a drive cycle, the ICE is forced to keep running for at least a certain amount of time before being deactivated. This is performed to enable warm up of the catalytic converter, which is essential to avoid high particle emissions during cold ICE cranking. In this work, the ICE is kept activated for at least 90 seconds after its first cranking since a stabilization in the particle number rate has been observed after this amount of time from the first ICE start in [13]. When the ICE is on, the ICE power P_{ICE} is set to a value interpolated from a one-dimensional lookup table with battery SOC as the independent variable. In general, ICE power is set higher for lower battery SOC. The controlled value of ICE torque can then be determined by dividing P_{ICE} by the instantaneous value of ICE angular speed. Once all the control variables are set (i.e. ICE on/off state and torque), the torque of the EM and the battery power can automatically be determined by considering the driver's torque demand and the controlled ICE torque. If the wheel power is negative (i.e. the vehicle is braking), the ICE is finally constrained to not deliver positive torque to improve the driving response of the vehicle. In this work, the RBC strategy is tuned to maintain the battery SOC within 18% and 22% when the HEV operates in charge-sustaining mode. Indeed, such narrow battery SOC range in charge-sustaining mode is calibrated to the large battery pack capacity of the retained plug-in HEV. In this work, a particle swarm optimization (PSO) algorithm is implemented to optimally tune the values of the control lookup table for P_{ICE}. The optimization target involves minimizing the overall HEV equivalent fuel consumption in a drive cycle, i.e. the actual fuel consumption plus the equivalent fuel consumption associated to the net battery energy consumption. The PSO is implemented in Matlab® software, while more details regarding the retained algorithm can be found in [14].

B. ECMS

In the retained HEV powertrain configuration, the ECMS operates at each time instant by selecting the value of T_{ICE} that minimizes the following cost function J_{ECMS}:

$$\arg\min[J_{ECMS}(T_{ICE})]$$

subject to:

$$J_{ECMS}(I_{batt} \geq 0) = \dot{m}_{fuel} \cdot LHV_{fuel} + \lambda_{dis} \cdot V_{OC} \cdot I_{batt}$$
$$J_{ECMS}(I_{batt} < 0) = \dot{m}_{fuel} \cdot LHV_{fuel} + \lambda_{cha} \cdot V_{OC} \cdot I_{batt} \quad (5)$$

where λ_{dis} and λ_{cha} are equivalence factors for the battery power in discharging and charging conditions, respectively, while LHV_{fuel} stands for the low heating value of the fuel in joules per gram. The equivalence factors weight the equivalent fuel consumption associated to the use of the high-voltage battery pack. In the traditional ECMS formulation, λ_{dis} and λ_{cha} are constant and they are tuned to comply with battery SOC constraints at the end of the drive cycle, i.e. to avoid excessive charge depleting [15]. In this work, a discretized vector is retained for the values of T_{ICE} ranging from 0 Nm to 270 Nm with an incremental step of 5 Nm, thus considering 55 elements in total. The ICE state is set to be activated in case the value of ICE torque that minimizes J_{ECMS} is greater than zero. As performed for the RBC strategy, the ICE is forced to be activated for at least 90 seconds after its first cranking.

C. A-ECMS (P control)

The A-ECMS differs from the traditional ECMS formulation since it considers values of λ_{dis} and λ_{cha} that vary over time instead of constant values. Furtherly improved HEV powertrain efficiency can be achieved in this way. Several adaptation laws can be implemented for the equivalence factors [15]. In this paper, two different equivalence factor adaptation laws are implemented for the A-ECMS. The first one is a proportional controller which adapts each equivalence factor over time based on the instantaneous value of battery SOC according to the following equation:

$$\lambda(t) = \lambda_0 + K_P \cdot \left[SOC_{ref} - SOC(t)\right] \quad (6)$$

where λ_0 and K_P are a constant term and the proportional coefficient for the generic equivalence factor λ which varies over time. Finally, SOC_{ref} stands for the reference value of the battery SOC, and its value is set here to 0.22 as this is the upper bound of the target battery SOC window. Here, λ_0 and K_P are tuned to achieve charge sustaining HEV operating conditions while maintaining the battery SOC within target values. Moreover, a further parameter is added in the A-ECMS formulation that forces the ICE to keep activated for a certain amount of time after each cranking event throughout the entire drive cycle. As it will be shown later in the results section, this is a crucial for keeping the frequency of ICE activations below a reasonable value not to deteriorate the comfort of the ride. This formulation of A-ECMS will be named *'A-ECMS (P control)'* moving on in the manuscript.

D. A-ECMS (table)

The second formulation of the A-ECMS implemented in this work is called *'A-ECMS (table)'*, This A-ECMS version differs from *'A-ECMS (P control)'* only concerning the law for adapting the values of equivalence factor as a function of the battery SOC. In *'A-ECMS (table)'*, two one-dimensional lookup tables are considered that respectively map the values of λ_{dis} and λ_{cha} as a function of the battery SOC. Here, the controlled values of equivalence factors as a function of battery SOC are calibrated using PSO in order to minimize the overall HEV energy consumption. Moreover, penalization terms are considered to avoid excessively frequent ICE de/activations over time and to prevent the battery SOC exceeding the retained allowed [0.18-0.22] window. These control strategy calibration criteria have been considered here when tuning the parameters of both *'A-ECMS (P control)'* and *'A-ECMS (table)'* using PSO.

For the sake of optimal calibration using PSO, the worldwide-harmonized light vehicle test cycle (WLTC) has been considered as target drive cycle for all the implemented HEV powertrain control strategies. Fig. 3 illustrates the value of parameters for both the RBC approach and the ECMS formulations as obtained by implementing PSO. For RBC and A-ECMSs, it can be noticed how respectively the controlled ICE power and the equivalence factors gradually increase as the battery SOC decrease. This allows achieving charge sustaining HEV powertrain operation without trespassing the boundaries of the allowed battery SOC window.

IV. Hardware-in-the-loop Assessment

In the previous sections, the HEV simulation platform was developed, and the HEV control strategies were implemented. This section describes the HIL assessment of the RBC approach and the ECMS formulations. Here, HIL tests are performed for two main reasons: 1) validating the effective execution of the real-time HEV powertrain control strategies on a real electronic control unit, and 2) measuring the on-board computational cost of the HEV powertrain control strategies. The HIL setup used in this work is described first. Then, obtained results are discussed.

A. HIL setup

Fig. 4 shows a picture and a schematic diagram of the HIL setup used in this work and installed at the Politecnico di Torino's Center for Automotive Research and Sustainable Mobility (CARS). The HIL setup includes: 1) a desktop computer that provides the user interface and allows the user to manage the HIL tests; 2) a dSpace Scalexio LabBox (DS 6001 type); 3) a dSpace MicroAutoBox (MAB) III (DS 1511 type). Looking at Fig. 2, HEV plant model, target drive cycle and driver sub-systems are flashed into the Scalexio LabBox, while a HEV control strategies is downloaded in the MAB before each HIL test is started. As displayed in Fig. 4(b), signals are exchanged between the MAB and the Scalexio LabBox through controller area network wiring (I/O CAN). The HEV simulation platform shown earlier in Fig. 2 can thus be implemented in the HIL setup.

B. Results

Fig. 5 shows HIL test results for all the implemented control strategies in terms of battery SOC, instantaneous fuel rate, and turnaround time. This latter parameter corresponds to the time required by the MAB to execute the workflow of the control strategy at each simulation time step. Here, the simulation time step for the HEV plant model and the other sub-systems downloaded in the Scalexio LabBox is set to 1 millisecond. The turnaround time over the entire WLTC displayed in Fig. 5 is always contained within 60 microseconds, which validates the effective execution of all

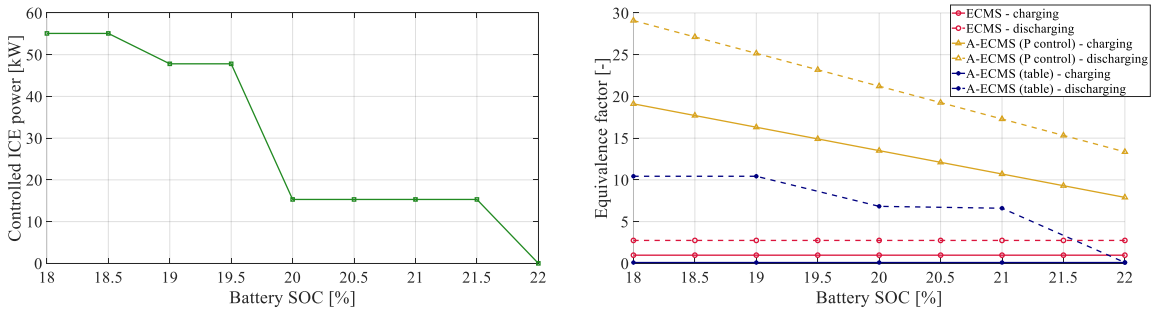

(a) RBC

(b) ECMS, A-ECMS (P control), A-ECMS (table)

Fig. 3. Calibrated parameters for the RBC approach and the ECMS formulations in terms of controlled ICE power and equivalence factors, respectively.

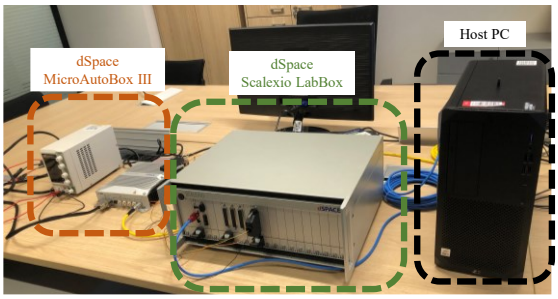

(a) HIL setup at the Politecnico di Torino - Center for Automotive Research and Sustainable Mobility (CARS)

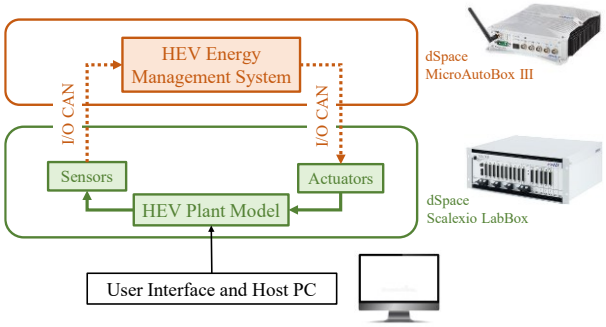

(b) Schematic diagram of the HIL setup

Fig. 4. HIL setup used in this work.

the implemented HEV control strategies on a real electronic control unit. Moreover, the lower the average turnaround time, the more efficient the HEV powertrain control strategy. Concerning the battery SOC time series illustrated in Fig. 5, all the HEV powertrain control strategy can comply with the considered SOC window boundaries except for ECMS. Indeed, ECMS is the only implemented HEV powertrain control strategy which is not calibrated to adequately limit the use of battery SOC window. On the other hand, both the A-ECMS formulations considered can fulfill the limitations imposed on the use of battery SOC window thanks to a dedicated methodology.

Fig. 6 illustrates statistics of the results obtained from the HIL tests for each HEV control strategy in terms of frequency of ICE activations over time, root-mean-square (RMS) of the ICE torque variation over time, average turnaround time and equivalent fuel economy. The RMS of the ICE torque variation over time particularly aims at assessing the comfort of the ride in terms of smoothness of the ICE torque. Concerning the frequency of ICE activations over time, the traditional ECMS exhibits poor comfort performance since it activates up to 70 times the ICE over the 30 minutes of the WLTC. On the other hand, both RBC and the A-ECMS formulations achieve improved performance by limiting the overall number of ICE activations below 6 over 30 minutes of driving. This corroborates the effectiveness of forcing the ICE to stay activated after being cranked in the A-ECMS formulations. When it comes to the RMS of the ICE torque variation over time, the RBC approach exhibits the lowest value by far. Again, ECMS is the worst performing strategy since entail an RMS of ICE torque variation more than 1.9 times higher compared with the RBC approach. On the other hand, both versions of A-ECMS can slightly limit the increase of ICE torque variation RMS: values for *'A-ECMS (P control)'* and *'A-ECMS (table)'* are indeed 1.7 times and 1.6

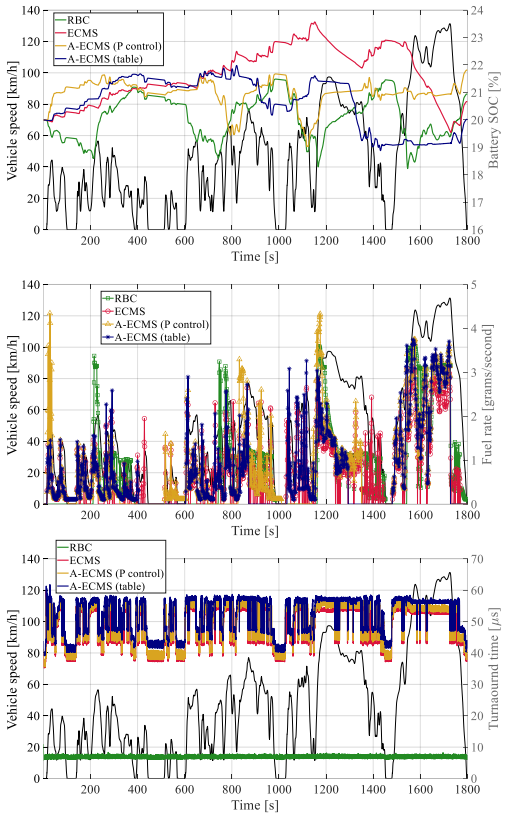

Fig. 5. WLTC time series of all the control strategies implemented in the HIL platform in terms in terms of battery SOC, fuel rate, and controller turnaround time.

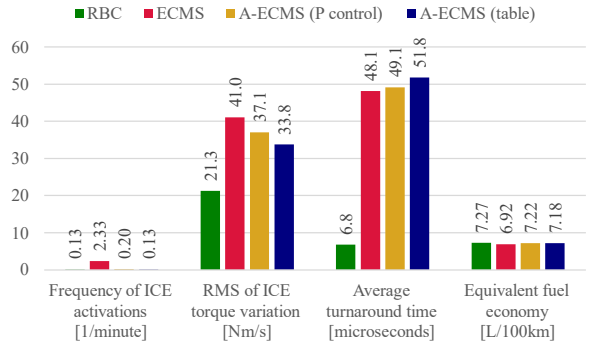

Fig. 6. Statistics of obtained results for the implemented HEV control strategies in terms of frequency of ICE ctivations, RMS of ICE torque variation, average turnarond time and equivalent fuel economy.

times higher compared with RBC, respectively. RBC exhibits the lowest computational effort as well: its average turnaround time is indeed one order of magnitude lower compared with both ECMS and the two A-ECMS formulations. Both *'A-ECMS (P control)'* and *'A-ECMS (table)'* entail slight computational cost increases of 2.0% and 7.5% compared with the baseline ECMS, respectively. These computational cost increases relate to the execution of the equivalence factor adaptation law in the MAB at each time instant. Looking at Fig. 5, the trend of the turnaround time for the RBC overall exhibits comparable values over time throughout the drive cycle. On the other hand, the turnaround time for both ECMS and A-ECMSs noticeably increases when the vehicle is moving. This relates to the calculation of the instantaneous cost function described in (5) being real-time executed in the MAB only if the vehicle speed or the driver's torque demand

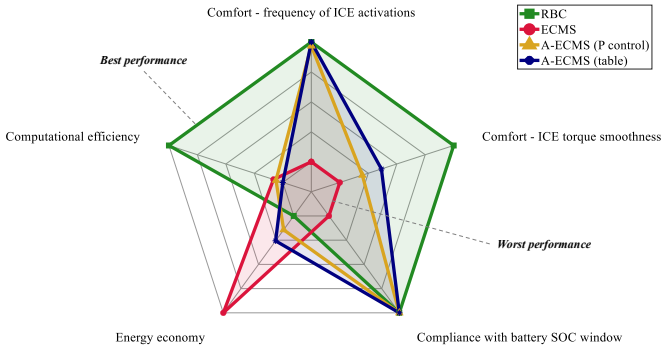

Fig. 7. Qualitative assessment of the HIL implemented HEV control strategies in terms of driving comfort, energy economy, compliance with battery SOC window and computational efficiency.

are greater than 0. Finally, when it comes to the equivalent fuel economy, the RBC is found underperforming with respect to ECMS and the A-ECMSs. Indeed, RBC consumes 5.1% more fuel compared to ECMS. On the other hand, *'A-ECMS (P control)'* and *'A-ECMS (table)'* preserve enhanced fuel economy by limiting the fuel consumption increase within 4.3% and 3.8% compared with ECMS, respectively.

V. Conclusions

HIL tests are crucial when selecting the most appropriate electrified powertrain on-board energy management strategy. In this paper, HIL tests are performed considering a parallel-through-the-road HEV powertrain. An RBC approach, the traditional ECMS formulation and two formulations of A-ECMS are implemented and benchmarked. Retained evaluation criteria include energy economy, computational efficiency, comfort level of the ride and compliance with the target battery SOC window. Fig. 7 summarizes the qualitative assessment of the HEV control strategies implemented in this work. RBC is currently the reference powertrain control approach in HEVs at industrial level. RBC can adequately meet all the considered HEV control objectives and requirements. However, it may be outperformed in terms of fuel economy. ECMS can remarkably improve the fuel economy of the considered HEV compared with RBC (i.e. up to around 5%). Nevertheless, this comes at the expenses of significantly worsening the on-board computational efficiency and failing all the retained battery SOC window compliance and comfort targets. A-ECMSs can mitigate the drawbacks of the ECMS in terms of battery SOC window compliance and comfort of the ride while preserving improved fuel economy. Nevertheless, they yield further worsening in the computational efficiency.

From a general perspective, this study suggests that implementing RBC approaches in HEVs may currently be advised when limited on-board computational power is a major concern. On the other hand, a formulation of the *'A-ECMS (table)'* may be suggested as a HEV fuel saving enabler when larger on-board computational power is available. Related future work could involve benchmarking the implemented control strategies with an off-line global optimal HEV control algorithm. Moreover, the implemented control logics could be tested by using the MAB as electronic control unit on-board a real HEV. Finally, next-generation HEV control strategies (e.g. of predictive type) could be developed, real-time implemented and benchmarked against the energy management approaches considered in this work.

References

[1] A. Biswas and A. Emadi, "Energy Management Systems for Electrified Powertrains: State-of-the-Art Review and Future Trends," in *IEEE Transactions on Vehicular Technology*, vol. 68, no. 7, pp. 6453-6467, July 2019.

[2] S. G. Wirasingha and A. Emadi, "Classification and Review of Control Strategies for Plug-In Hybrid Electric Vehicles," in *IEEE Transactions on Vehicular Technology*, vol. 60, no. 1, pp. 111-122, Jan. 2011.

[3] A. Biswas, P. G. Anselma and A. Emadi, "Real-time Optimal Energy Management of Multi-mode Hybrid Electric Powertrain with Online Trainable Asynchronous Advantage Actor-Critic Algorithm," in *IEEE Transactions on Transportation Electrification*, in press, 2022.

[4] Y. Li and B. Chen, "Development of integrated RBC and equivalent consumption minimization strategy for HEV energy management," *2016 12th IEEE/ASME International Conference on Mechatronic and Embedded Systems and Applications (MESA)*, pp. 1-6, 2016.

[5] A. Biswas, P. G. Anselma, A. Rathore and A. Emadi, "Comparison of Three Real-Time Implementable Energy Management Strategies for Multi-mode Electrified Powertrain," *2020 IEEE Transportation Electrification Conference & Expo (ITEC)*, 2020, pp. 514-519.

[6] R. Mura, V. Utkin and S. Onori, "Energy Management Design in Hybrid Electric Vehicles: A Novel Optimality and Stability Framework," in *IEEE Transactions on Control Systems Technology*, vol. 23, no. 4, pp. 1307-1322, July 2015

[7] A.E. Hartavi, I.M.C. Uygan, L. Güvenç, "A hybrid electric vehicle hardware-in-the-loop simulator as a development platform for energy management algorithms", in *International Journal of Vehicle Design*, vol. 71, no. 1-4, pp. 410-429, 2016.

[8] V. I. Herrera, A. Milo, H. Gaztañaga, A. González-Garrido, H. Camblong and A. Sierra, "Design and Experimental Comparison of Energy Management Strategies for Hybrid Electric Buses Based on Test-Bench Simulation," in *IEEE Transactions on Industry Applications*, vol. 55, no. 3, pp. 3066-3075, May-June 2019.

[9] Fiat Chrysler Automobiles, "Renegade 4xe and Compass 4xe: the Jeep® brand's take on the plug-in hybrid," http://www.media.fcaemea.com/em-en/jeep/press/renegade-4xe-and-compass-4xe-the-jeep-brand-s-take-on-the-plug-in-hybrid (accessed 11 January 2022).

[10] United States Environmental Protection Agency, "Data on Cars used for Testing Fuel Economy", [online] https://www.epa.gov/compliance-and-fuel-economy-data/data-cars-used-testing-fuel-economy (accessed 11 January 2022).

[11] J. Dabadie, A. Sciarretta, G. Font, F. Le Berr, "Automatic Generation of Online Optimal Energy Management Strategies for Hybrid Powertrain Simulation," *SAE Technical Paper* 2017-24-0173, 2017.

[12] M. Duoba, H. Lohse-Busch, R. Carlson, T. Bohn et al., "Analysis of Power-Split HEV Control Strategies Using Data from Several Vehicles," *SAE Technical Paper* 2007-01-0291, 2007.

[13] H. Badshah, D. Kittelson, W. Northrop, "Particle Emissions from Light-Duty Vehicles during Cold-Cold Start," *SAE Int. J. Engines*, vol. 9, no. 3, pp. 1775-1785, 2016.

[14] P.G. Anselma, "Optimal adaptive race strategy for a Formula-E car", *Proceedings of the Institution of Mechanical Engineers, Part D: Journal of Automobile Engineering*, 2021.

[15] F. Zhang, K. Xu, L. Li and R. Langari, "Comparative Study of Equivalent Factor Adjustment Algorithm for Equivalent Consumption Minimization Strategy for HEVs," *2018 IEEE Vehicle Power and Propulsion Conference (VPPC)*, 2018, pp. 1-7.